Available online at www.CivileJournal.org

Civil Engineering Journal

(E-ISSN: 2476-3055; ISSN: 2676-6957)

Vol. 11, No. 06, June, 2025

Influence of Resistance Spot Welding Parameters on Cold-Formed Steel Properties and Failure Modes

Iosif Hulka [1], Viorel Ungureanu [2, 3*], Ioan Both [2], Edward Petzek [2], Bogdan Radu [4]

[1] *Research Institute for Renewable Energies, Politehnica University Timişoara, G. Muzicescu 138, 300501 Timişoara, Romania.*

[2] *Department of Steel Structures and Structural Mechanics, Politehnica University Timişoara, Ioan Curea 1, 300224 Timişoara, Romania.*

[3] *Romanian Academy, Timişoara Branch, Mihai Viteazu 24, 300223 Timişoara, Romania.*

[4] *Department of Materials and Manufacturing Engineering, Politehnica University Timisoara, Timişoara 300222, Romania.*

Received 22 October 2024; Revised 14 May 2025; Accepted 21 May 2025; Published 01 June 2025

Abstract

Lightweight steel structural systems such as built-up beams and trusses are efficient and easy to handle, but the joining technique between thin-walled cold-formed steel elements requires improved solutions. Conventional welding technologies are not suitable for connecting thin sheets due to several inconveniences. The study presents a novel technological approach to connect lightweight steel beams made of corrugated galvanised sheets for webs and back-to-back lipped channel profiles for flanges connected by spot welding, as resistance spot welding (RSW) is widely used in various industrial sectors, such as automotive. This study investigates the influence of RSW parameters on the microstructural properties of spot-welded low-carbon galvanised steel sheets, as well as on their mechanical properties. Two grades of base material were used with thicknesses in the range of 0.8 - 2 mm. RSW joints were manufactured using an automated welding source, and their microstructural characteristics were evaluated by optical and electron microscopy to emphasise the importance of using optimal welding regimes to reduce weld failure. Mechanical properties were evaluated using Vickers microhardness measurements and nanoindentation. Tensile tests were carried out to assess the force-displacement curves and identify the failure mode. The results of the study show that RSW is a promising method for fabricating lightweight steel structural systems when the current, time, and interelectrode forces of RSW are carefully selected.

Keywords: Lightweight Steel Structures; Built-Up Beams and Trusses; Resistance Spot Welding; Microstructure; Hardness.

1. Introduction

Thin-walled cold-formed steel structures have emerged as a key innovation in modern constructions, offering a combination of economic efficiency, structural integrity, and sustainability. These lightweight structures are especially suited for a range of applications, from residential buildings to commercial or industrial ones. In the construction industry, thin-walled cold-formed steel structures are widely used, either in conjunction with hot-rolled or fabricated steel profiles or as standalone structures for low- to mid-rise constructions. Using lightweight elements, this can be achieved with good strength-to-weight ratios. It is necessary to reduce weight without compromising human safety. The economic advantages of thin-walled cold-formed steel structures are substantial. Their lightweight nature allows for reduced transportation costs and simplified foundation requirements, leading to faster construction timelines. Additionally, as a sustainable building material, cold-formed steel is recyclable and can contribute to greener building standards. As the industry focuses on efficient and environmentally responsible practices, thin-walled cold-formed steel structures stand out as a viable solution to the challenges of modern architecture.

* Corresponding author: viorel.ungureanu@upt.ro

http://dx.doi.org/10.28991/CEJ-2025-011-06-01

One of the notable features of these structures is their zinc layer protection, which provides exceptional corrosion resistance, extending the lifespan of steel components and reducing maintenance costs. Moreover, cold-formed steel (CFS) sections have limited capacity due to their instability limitations, and one way to enhance their strength and performance is to manufacture built-up members. The incorporation of built-up members, comprised of multiple thin-walled sections, further enhances the strength and stability of the structures, making them capable of withstanding significant loads while maintaining a minimal material footprint.

A built-up member with discrete connections along the length may experience failure of the individual members or buckling in interaction modes depending on the intermediate connection type, spacing, and slenderness. Commonly connected by self-drilling screws or bolts, the rigidity of such a connection is small; thus, there is a need for a more rigid fastening (such as bolts or welding) that is more consistent in terms of repeatability. A solution to enhance the performance of thin-walled cold-formed steel structures could be the use of resistance spot welding (RSW) to join different elements made entirely from thin sheets. Their design leverages spot welding techniques, which not only ensure secure joints but also promote faster and more efficient assemblies.

The resistance spot welding of thin galvanised elements is a common technique most often encountered in the automotive sector, where it is employed because of its high productivity, low cost, and enhanced labour efficiency. By using RSW, advanced high-strength steels with lower weldability can be welded alongside traditional steels [1] without the need for any other filler material to form the weld. The process involves joining overlapping steel sheets by applying pressure and heat from an electrical current to form a weld at the interface with well-established process parameters to ensure the reliability and quality of the joints. To achieve high-quality resistance spot welds, a careful balance of current, time, electrode force, and consideration of the properties of the material being processed is required. Proper parameter optimisation ensures the desired microstructure and mechanical characteristics, which contribute to the overall performance and reliability of the structure. While the uncoated steel sheets can be easily welded, galvanised sheets with Zn-based protective coatings are a major challenge and require special handling to ensure consistency and reliability in production. Welding galvanised steel introduces challenges due to the zinc layer, which can lead to defects such as liquid metal embrittlement (LME) and brittle intermetallic formations. If the welding parameters are well selected, the method deals with even the complications that can occur during welding, such as LME induced by the zinc-coated steel sheet surface [2]. These issues highlight the need for precise control over welding parameters, including current, time, and electrode force, to ensure quality joints. Additionally, the shape and cooling rate of the weld influence microstructure evolution and mechanical behaviour.

Thin-walled cold-formed steel, known for its high strength and formability, requires precise welding parameters to avoid issues such as burn-through or insufficient fusion. If galvanised sheets are used to manufacture them, the zinc coating offers corrosion resistance, but it can complicate welding by introducing additional elements and potentially forming brittle intermetallic compounds within the weld. To avoid such problems, in addition to optimising the RSW parameters, it is necessary to select the correct electrode shape, which requires special attention since:

- High welding currents can cause burn-through, distortion, or expulsion of molten material, while low currents may result in inadequate fusion and weak welds;
- Longer welding times increase heat input, potentially enhancing fusion, but posing risks of overheating and material degradation, while shorter times may not provide sufficient heat for proper weld formation;
- Proper contact and heat generation at the weld joint requires adequate force, as too much can cause material indentation or thinning, while too little can result in poor electrical contact;
- The shape and size of an electrode significantly influence its heat distribution and pressure application; common geometries are flat, domed, or truncated;
- Rapid cooling enhances mechanical properties by achieving a fine-grained microstructure, while controlled cooling prevents the formation of brittle phases.

The welding parameters influence the microstructure of the joint, which changes during RSW. Depending on them and the cooling rate, the fusion zone (FZ) may contain martensitic or ferrite/bauxite phases, while the heat-affected zone (HAZ) experiences thermal cycles. In addition, an advantage of the processes is that the base metal (BM) remains unaffected. All the process parameters affect not only the microstructure but also the mechanical properties of the welded joint. Among them, the most important mechanical properties are tensile strength, hardness, and ductility. Therefore, optimal welding parameters result in a strong weld that is comparable to or exceeds the strength of the base metal and ensures that the joint can accommodate some plastic deformation. If the parameters are not well selected, weld failure may occur. Weld failure includes several modes such as: (i) pull-out failure; (ii) interfacial failure and (iii) button-pull failure. These failures are caused by insufficient weld nugget size, poor fusion, insufficient heat input, the presence of brittle intermetallic compounds, or inadequate weld strength. Therefore, process optimisation, determined by trial-and-error or empirical formulas, is critical in RSW.

2. Literature Review

Resistance spot welding (RSW) remains an important technique for joining galvanised thin-walled cold-formed steel elements, especially in sectors prioritising lightweight and high-strength structures. Recent studies have expanded the understanding of the microstructural and mechanical implications of RSW, particularly in relation to galvanised coatings, dissimilar material joints, and process monitoring.

Adkine & Biradar [3] provided a comprehensive review of resistance spot welding (RSW), emphasising its critical role in industrial applications such as automotive and aerospace manufacturing due to its efficiency and reliability. The study explores how key parameters—such as welding current, time, and pressure-interact with material properties to influence weld quality. Special attention is given to RSW of dissimilar materials, where metallurgical transformations and mechanical behaviours are highly sensitive to parameter selection. The review highlights recent advances in optimising welding conditions to improve microstructural characteristics and mechanical performance, offering strategic guidance for enhancing manufacturing processes and innovation in RSW technology.

Rao et al. [4] presented a study that examined the associated changes in shear strength and monitored the dynamic contact resistance during the welding process, while analysing the corresponding variations in the resistance parameters of the spot-welding process to determine the appropriate nugget growth parameters. They also analysed the transition of failure modes in response to different process parameters. A critical nugget diameter was experimentally determined, distinguishing between interfacial and pull-out failure modes, using failure mode analyses. Different numerical models were evaluated for the estimation of the diameter of the critical nugget to optimise the RSW parameters.

Biradar & Dabade [5] attempted to understand the effect of welding parameters on joint strength and quality. Experimental tests were carried out on mild steel and austenitic stainless steel to understand the change in joint characteristics and properties to achieve better weld quality. Viňáš et al. [6] show the results of galvanised micro-alloyed steel sheets used in the construction of automobile bodies that were welded using RSW. After using different welding currents and welding times, they concluded that these are the main ones that influence the quality of spot welds when the same pressing force was applied. Emre & Kaçar [7] investigated the RSW of galvanised and bare TRIP800 sheet steels. They also investigated the effect of the RSW time and current on the joint microstructure and mechanical properties. It became clear that the martensitic transformation caused the hardness to increase in both the fusion zone and the heat-affected zone (HAZ) of both the galvanised and the TRIP800 joints. Furthermore, it turned out that the welded joint manufactured using galvanised sheets had a somewhat greater hardness in HAZ. This is due to the formation of finer grains, leading to increased hardness because the protective zinc coating accelerates heat conduction and prevents the grains from coarsening in HAZ. Hamidinejad et al. [8] simulated and optimised the RSW process parameters for bake-hardenable and interstitial-free galvanised steel sheets used in the automotive industry. The parameters of the RSW process were determined using a genetic algorithm technique, resulting in an improved tensile-shear strength in agreement with the real experimental data.

The mechanical tests conducted by Chao [9] revealed the failure mechanisms of RSW joints in lap shear and cross-tension tests. From these observed failure patterns, the stress distribution was deduced, leading to the development of a theoretical model for mixed normal and shear loading conditions. Radakovic & Tumuluru [10] used numerical simulation to determine the durability of RSW joints, identify failure modes and assess the impact of shear testing on high-performance steels. Their research confirmed two failure mechanisms: interfacial fracture and complete button pull-out. Their study indicates that failure mode alone should not be the sole criterion for evaluating spot weld quality. Instead, when interpreting the results of the shear-tension tests, the focus should be on the load-bearing capacity as well. Pouranvari et al. [11] developed an analytic model to predict the failure mode of RSW joints. According to their research, the metallurgical characteristics of the welds must also be taken into account to achieve a more accurate prediction and analysis of the joint failure mode.

In addition to RSW, attempts were made to create similar joints between thin galvanised steel sheets by using laser technology. Miyazaki & Furusako [12] studied tensile shear testing to determine the maximum load and location of the fracture of the laser-welded lap joints. Based on the experimental results a mechanical prediction model was developed. Furthermore, Landolfo et al. [13] conducted a comprehensive experimental study on laser welded joints, evaluating the effects of laser welding parameters on thin sheets using both lap shear and tensile tests. In addition to laser welding, Kodama et al. [14] also used arc welding techniques, with a focus on automotive components manufactured using high-strength steel. The application of the cold metal transfer process has been shown to enhance both the static and fatigue strength of the welded joints.

In RSW, selecting the appropriate technology requires equipment capable of controlling key parameters such as force, time, and current. In addition, users must consider the diameter of the electrode tip diameter, as variations in sheet thickness and these factors significantly impact the quality of the spot weld [15].

The RSW parameters influence both the expulsion of the zinc from the surface of the galvanised sheets and the weld strength [16]. If higher currents are used, they can lead to significant zinc expulsions and weaken the joint strength [17]. This was revealed by microscopic studies performed by Chao [9], who demonstrated how the loading condition (whether

it be tensile, shear, or mixed tensile/shear loads) is influenced by microstructural characteristics. Besides, the base materials play a significant role. Thus, dissimilar spot welds, such as those between steel and stainless steel [18] or between galvanised sheet and aluminium alloy [19], have been the subject of microstructural studies. Majlinger et al. [20] proposed new equations to predict the shear and cross tension strength, which can be used to plan within the 300-1890 MPa range of tensile strength of the base metals for similar and different RSW joints of thin steel sheets.

Liquid Metal Embrittlement (LME) continues to challenge the integrity of RSW joints in zinc-coated advanced high-strength steels. Yang et al. [21] compared Zn-Al-Mg and traditional galvanised coatings, revealing that Zn-Al-Mg coatings exhibit reduced LME susceptibility due to their distinct metallurgical interactions during welding. Additionally, research reveal that the effect of LME cracks in reducing load-bearing capacity is more pronounced under impact loading than under quasi-static loading, highlighting a previously underexplored aspect of LME behaviour under impact loading [22]. A 2024 study on tensile-shear fatigue of Zn-coated AHSS joints found that despite the presence of LME cracks, fatigue life was not significantly reduced compared to bare steel, suggesting that fatigue cracks initiate primarily at high-stress zones rather than LME sites [23].

Joining dissimilar materials, such as aluminium and steel, poses challenges due to differing thermal and mechanical properties. Innovative approaches, like incorporating cold-gas-sprayed (CGS) inlayers, have shown promise. Hagen et al. [24] demonstrated that CGS inlayers facilitate metallurgical bonding between aluminium and steel, enhancing joint strength and mitigating defects. Similarly, the use of copper/nickel interlayers has been explored to control intermetallic compound formation in aluminium-steel joints, improving weld quality [25]. In 2024, the application of preheating currents was shown to expand the expulsion-free window in dissimilar joints, reducing thermal shocks and improving process control [26]. Ensuring consistent welding quality necessitates effective process monitoring. Ullrich et al. [27] introduced electrode displacement monitoring as a real-time quality assurance method for RSW of galvanised dual-phase steels, enabling early detection of weld anomalies and correlation with nugget geometry. Additionally, studies on pre-pulse RSW techniques have focused on extending electrode life expectancy, particularly when welding coated high-strength interstitial-free steels, by analysing dynamic resistance and temperature profiles [28].

Investigations into the weldability of twinning-induced plasticity (TWIP) steels revealed that the heat-affected zone (HAZ) often becomes the weakest link due to grain coarsening and manganese carbide formation, leading to brittle fracture modes [29]. These findings underscore the importance of controlling thermal inputs to preserve joint integrity. Complementary finite element modelling efforts have further elucidated stress and strain distributions in tensile shear RSW joints in galvanised steels, providing a predictive framework for design optimisation [30].

A comprehensive review highlighted the intricate relationship between welding parameters, metallurgical transformations, and mechanical behaviours in RSW, especially concerning dissimilar material joints. The review emphasised the need for optimised parameter selection and advanced monitoring techniques to enhance weld quality [3, 31].

Despite these advancements, several areas warrant further exploration:

- Standardisation of RSW Parameters: There is a lack of standardised guidelines for RSW parameters when dealing with emerging coatings like Zn–Al–Mg, which affects reproducibility and quality assurance;
- Long-Term Performance Studies: Limited data exist on the long-term durability and fatigue performance of RSW joints in dissimilar material combinations, particularly under varying environmental conditions,
- Integration of Real-Time Monitoring: While methods like electrode displacement monitoring show promise, their integration into industrial settings for real-time quality control remains underdeveloped.

Taking into account the high interest in RSW of thin sheets, the present study is a continuation of the research within the WELLFORMED project funded by the Executive Agency for Higher Education, Research, Development and Innovation Funding (UEFISCDI), where an extensive trial was conducted using tensile shear tests on RSW lap joints. Various sheet thicknesses were used for the experimental part of the project and combined using RSW, followed by tests on individual joints and on full-scale beams to evaluate their performance [32].

Addressing the gaps found in the literature and the need to deepen the research in this field, the present study offers a detailed experimental evaluation of RSW joints in built-up thin-walled cold-formed steel beams, focusing on (1) Realistic material combinations (S250GD and S350GD grades); (2) Microstructural and mechanical analysis of lap joints across various thicknesses; (3) Evaluation of nugget formation, failure modes, and Zn-related effects at both micro and macro levels. This contributes new insights into how RSW can be optimised for construction-specific applications, enabling more reliable and lightweight steel assemblies. This study presents an interdisciplinary approach that combines steel construction, welding technology, and materials science, bringing added value to a practical application relevant to today's needs, in which we focus on optimising the use of limited material resources through the use of a relatively new solution based on specially designed thin sheets joined by RSW.

Moreover, the present work aims to show how the RSW process parameters affect the mechanical properties and macro- and microstructure of joints used to manufacture built-up thin-walled cold-formed steel beam components made from low carbon galvanised steel sheets. The experimental part of the study, results, and discussions are structured as follows: Section 3 describes the materials and methods used in the experimental investigation, including details of the resistance spot welding (RSW) process and setup, material specifications, and testing procedures; Section 4 presents the results of microstructural and mechanical analyses, followed by a detailed discussion of nugget formation, hardness distribution (Vickers microhardness and nanoindentation), tensile performance, and failure mechanisms. Finally, Section 5 concludes the paper by summarising the key findings and highlighting the practical implications of the study, as well as potential directions for future research. Thus, the study aims to gather valuable information for the design of novel thin-walled cold-formed steel structures.

3. Material and Methods

The research result of the WELLFORMED project consists of structural elements with high efficiency due to material savings, having three components made of thin galvanised steel sheets, i.e. flanges (lipped channel section profiles), shear panels (flat sheets), and corrugated web (trapezoidal corrugated sheet) as presented in Figure 1, connected by RSW.

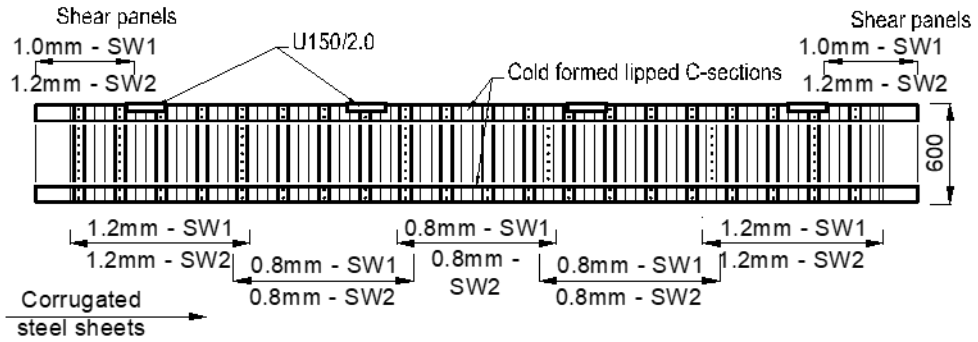

Figure 1. Schematics of built-up beam composed of thin-walled cold-formed elements [32]

Two beams with a span of 5.157 m and a height of 0.6 m were fabricated for the full-scale tests. The manufacturing process consists of the following 4 main steps: (i) joining the corrugated galvanised sheets for the web, (ii) joining the shear plates at the ends of the beam, (iii) joining the top and bottom flanges, and (iv) joining the end parts of the beam to ensure a rigid connection to the test stand. Six M12 grade 8.8 bolts were used to connect each flange to the mild steel assembly. Six bolts were installed at the height of the shear panel to secure the shear panel to the support assembly. The beams were loaded using a lever system that distributed the actuator force in 4 points according to a monotonic protocol with a loading speed of 2 mm/min.

The deformation after the test of a representative beam is shown in Figure 2-a. The failure mode of the beam started with the buckling of the shear panel (Figure 2-b), followed by the distortion of the corrugated web (Figure 2-c), and after reaching the maximum force, some RSW joints were observed to fail by nugget pull-out (Figure 2-d). The behaviour of the beam was ductile, and the collapse occurred at a displacement of approximately 123 mm.

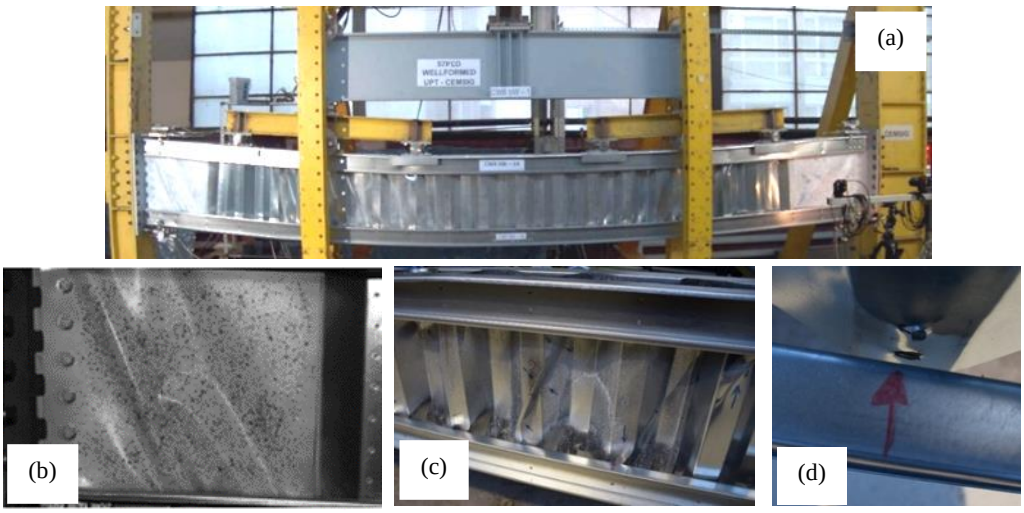

Figure 2. Built-up beam after the test: a) global deformation during the test, b) shear buckling, c) distortions of the corrugated web and d) nugget pull-out [32]

To thoroughly investigate and understand the response of the full-scale beams manufactured from thin-walled cold-formed steel welded using RSW, the experimental tests of the present study consisted of making lap joints using combinations of different sheet thicknesses and investigating their microstructure and mechanical properties, such as hardness and tensile-shear tests. Given the varying thicknesses of these cold-formed steel components, it is crucial to perform an in-depth analysis of the performance of the connections between galvanised steel sheets.

Figure 3 presents a flowchart illustrating briefly the workflow and methodology used in the present study.

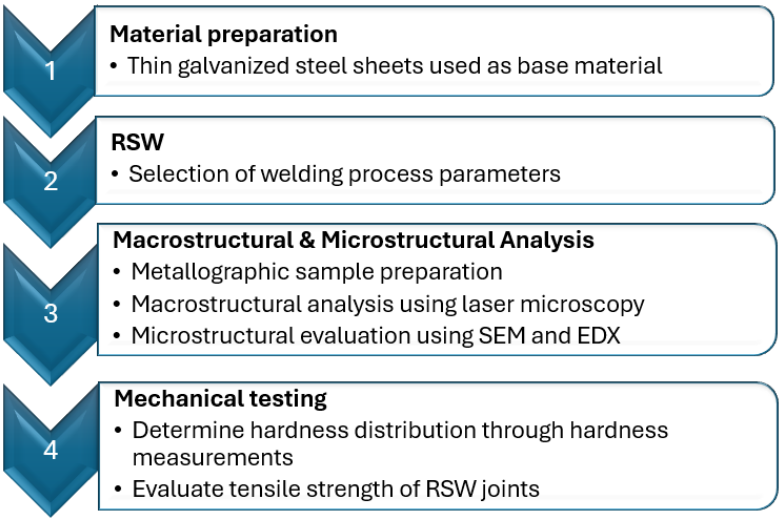

Figure 3. Flowchart presenting the workflow and methodology

3.1. Base Materials

The base materials used for the experimental part of the present work were commercially available S250GD and S350GD grade sheets. The steel sheets varied in thickness as follows: 0.8 mm and 1.2 mm for the S250GD grade and 2 mm for the S350GD grade. According to the manufacturer the chemical composition of the sheets is as follows: C ≤ 0.2 wt.%, Si ≤ 0.6 wt.%, Mn ≤ 1.7 wt.%, P ≤ 0.1 wt.% and S ≤ 0.045 wt.%.

3.2. Sample Fabrication

Figure 4 presents the RSW process consisting of four stages: (i) the squeeze cycle – when the top copper electrode is brought into contact with the base material and a force is applied to the weld area; (ii) weld cycle – the current is turned on and the resistance to current flow at the sheet interface results in the formation of a nugget; (iii) the dwell cycle - the current is turned off and the nugget cools down gradually and solidifies under continuous pressure; and (iv) the off cycle - is the final step of the process when the copper electrode is raised from the surface of the sheet [33]. During the process, the copper electrodes are permanently cooled down with water. To prepare the RSW joints, an Inverspotter 1400 Smart Aqua (Telwin, Villaverla, Italy) welding equipment with DC inverter was used combined with automatic parameter setting technology. The equipment can control the welding parameters in terms of welding current, time, and the force between the electrodes.

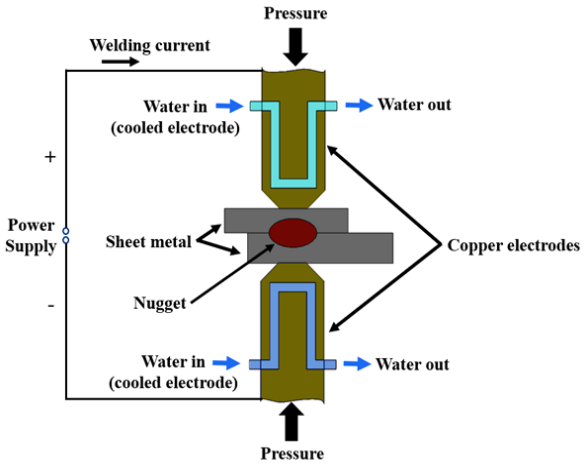

Figure 4. Spot welding process

Table 1 presents the RSW parameters: (i) welding current Is (A), (ii) time t (ms), and (iii) the force between the electrodes F (N), as well as the thickness (t) of the sheets employed in the study.

Table 1. RSW parameters and sheet thickness

Parameter / Sample	I_s [A]	F [N]	t [ms]	t_1 [mm]	t_2 [mm]	R_{total} [μΩ]	Q [J]
Sample 1	9812	4300	446	0.8	2	101.3	4349.70
Sample 2	9472	3650	405	0.8	2	101.3	3680.85
Sample 3	9627	4150	439	0.8	2	101.3	4121.51
Sample 4	9989	4670	461	0.8	2	101.3	4659.66
Sample 5	10248	5150	458	1.2	2	101.5	4882.13
Sample 6	10663	4880	473	1.2	2	101.5	5458.66

3.3. Cross-sectional Analysis

Metallographic analysis was performed to study the macro and microstructure of the RSW joints. To achieve a mirror-like surface, the samples were polished with a 0.3 μm diamond-based suspension after grinding with SiC abrasive papers with grit sizes up to 4000P. After a 5% Nital reagent etch was performed to reveal the joint structure. A schematic representation of an RSW joint is presented in Figure 5 with specific annotations.

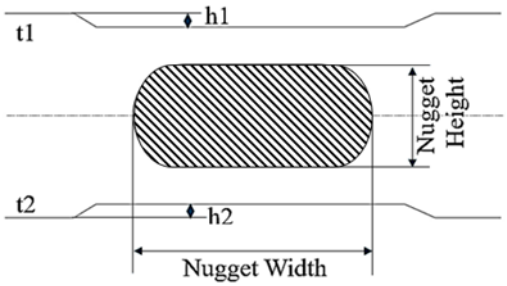

Figure 5. Cross-sectional representation of the weld nugget where t_1 (0.8 mm and 1.2 mm) and t_2 (2 mm) are the base materials with different thicknesses, h_1 and h_2 the indentation depth

The geometry of the nugget and microstructure of the samples were examined using an Olympus Lext OLS4000 confocal microscope (Olympus, Tokyo, Japan).

Scanning electron microscopy (SEM: Quanta FEG 250, FEI, OR, USA) with a backscattered electron detector (BSD) was used to study the microstructure of the samples at higher magnification. X-ray dispersive spectroscopy (EDX) was used for elemental analysis (Apolo SSD detector, EDAX Inc. NJ, USA).

Microhardness testing was conducted with a ZHVμ hardness tester (Zwick/Roell, Ulm, Germany) based on the Vickers method using a load of 100 gram-force and a dwell time of 15 s. A number of 10 indentations were made on each base material in the cross-section.

Three distinct areas were subjected to nanoindentation: the base materials, the heat-affected zone, and the nugget. A number of nine measurements were performed on each area and the elastic modulus and hardness were extracted from the results. For the measurements, a Nano-hardness Tester (NHT, Anton Paar, Graz, Austria) was used. The Berkovich indenter was employed using linear loading with a maximum load of 30 mN. The loading rate was 60 mN/min with an approach distance of 2000 nm and a pause of 15s. The measurements were performed on metallographic samples with mirror-like surfaces.

3.4. Tensile Test

Using a Zwick universal testing machine (Zwick/Roell, Shanghai, China), tensile tests were performed on lap joints made from various combinations of sheet thicknesses. The deformation was recorded using a contact extensometer with a gauge length of 80 mm and a speed of 3 mm/min, which is similar to the loading rate specified in ISO 6892-1:2019, Metallic materials - Tensile testing. The machine's load cell tracked the loading. Figure 6 presents the design of one sample prepared for the tensile-shear test. Prior SEM investigations, the samples were cleaned with ethanol in an ultrasonic bath to remove contaminants after tensile tests.

Figure 6. RSW sample prepared for tensile test

4. Results and Discussions

4.1. Microstructure of Base Material

Figure 7 shows the microstructure of the undeformed base materials in the longitudinal direction, from which it can be observed that the microstructure is characterised by equiaxed grains with different shapes and sizes depending on the steel grade and thickness. The base material has a predominantly ferritic structure (ferrite grains, with perlite at the edge of the ferritic grains), typical for hypoeutectoid steel. The average grain size was calculated using the line intercept method and the results showed that the 0.8 mm sheet had 11.95 µm, the 1.2 mm sheet had 8.81 µm, while the 2 mm sheet had 5.59 µm. According to the hardness measurements, (i) the 0.8 mm sheet had an $HV_{0.1}$ of 107.8; (ii) the 1.2 mm sheet had an $HV_{0.1}$ of 115.2; and (iii) the 2 mm sheet had an $HV_{0.1}$ of 140.1. In addition to chemical composition, grain size is a major contributor to the hardness of base materials. As a result, it was found that smaller grains lead to higher hardness, as a consequence of the effect of the grain boundaries on the sliding of crystallographic planes.

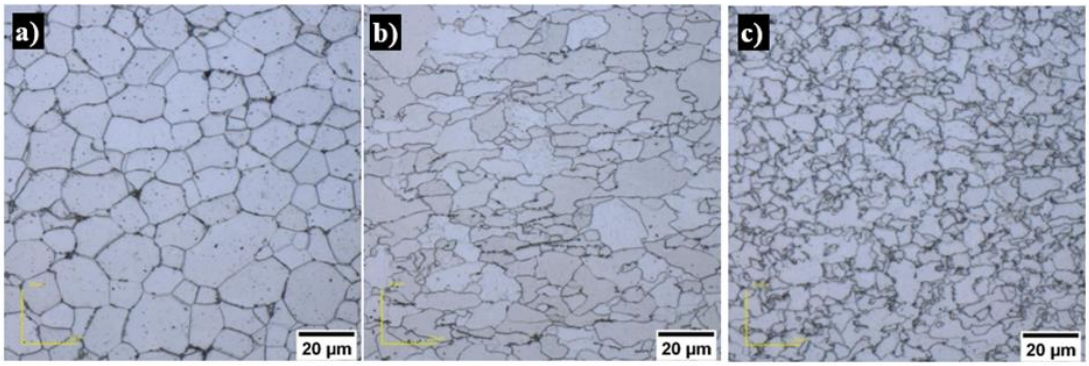

Figure 7. Microstructure of low carbon sheets used in the experiment: a) S250GD of 0.8mm; b) S250GD of 1.2 mmand c) S350GD of 2 mm

4.2. Nugget Geometry

Figure 8 shows the typical macrostructure of RSW joints. The weld region is comprised of three main structural zones, revealed by the etchant, which are: (i) the base metal (BM), (ii) the heat affected zone (HAZ), and (iii) the nugget zone (FZ).

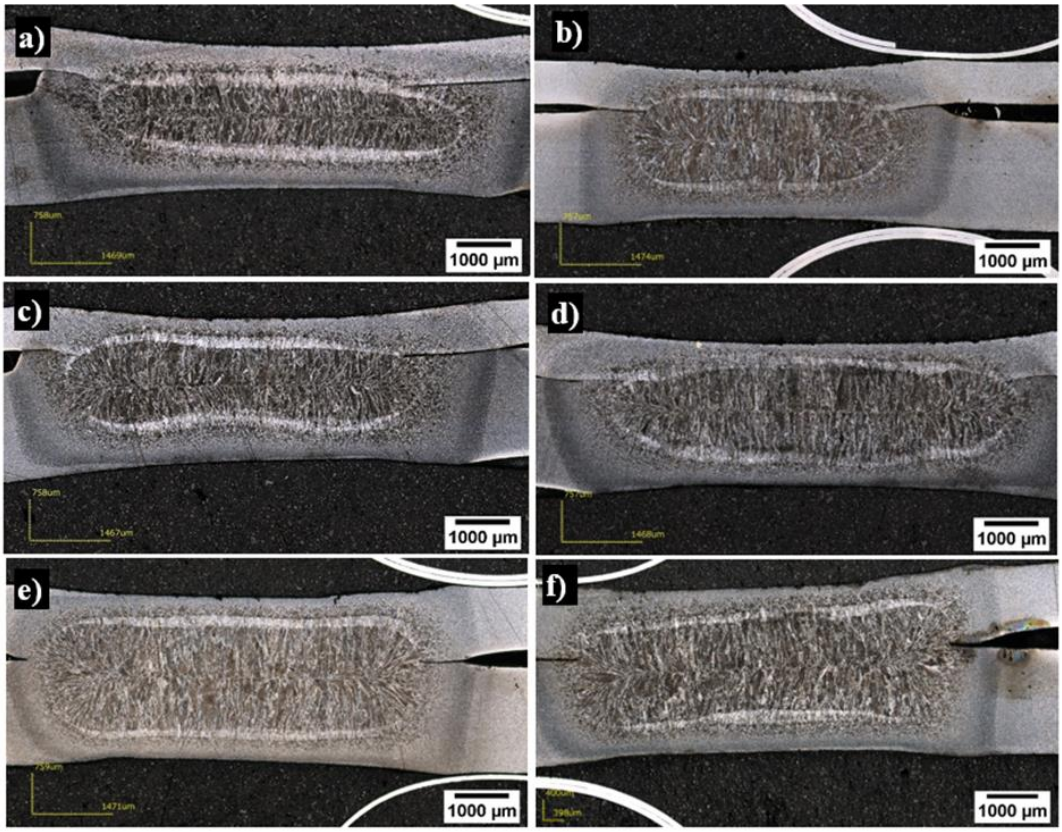

Figure 8. Overall macrostructure of weld nuggets geometry in cross-section: a) Sample 1; b) Sample 2; c) Sample 3; d) Sample 4; e) Sample 5 and f) Sample 6

During RSW, the material in the nugget melts and resolidifies, resulting in the formation of a cast structure characterised by columnar grains that elongate along the cooling direction. Heat cycling causes HAZ to undergo microstructural changes rather than melting during the welding process [9]. In all RWS joints, it can be observed that there are no macroscopic defects such as pores, cavities, or cracks within the fusion or heat-affected zones. However, there are differences in the nugget geometry due to the RSW parameters, which varied slightly according to surface quality, cleanliness, and thickness of the sheets employed in the experiment. It is well known that a high heat input would increase the weld deformation, as would be expected from an increased depth of penetration of the electrode into the base material. This contributes to the formation of a larger nugget while reducing the unmelted sheet area between the fusion zone and the electrode [34]. This is highlighted by the macrostructure of Sample 2, welded using a welding current of 9472 A. From the observations, the lowest current leads to the lowest nugget width. Kianersi et al. reported similar findings in their study, which was attributed to insufficient heat input that caused nugget formation with smaller dimensions [35]. This might be attributed to an insufficient force or imperfect contact between the electrodes. In comparison, Sample 6, welded using the highest welding current employed to weld 0.8 mm and 1.2 mm sheets, presents an increased width of the nugget geometry, which is in line with the theoretical aspects.

To evaluate the influence of process parameters on nugget geometry, measurements were performed on the macrostructures presented in Figure 8, and the results are summarised in Table 2. In both sets of samples, it was observed that as the value of the welding current increases, the diameter of the nugget increases as well. The growth of the nuggets relies on the welding current based on Joule's law [36]. The indentation depth in the samples was somewhat deeper in the thinner sheet, while the footprint was smaller in the thicker sheet due to the higher hardness of the galvanised sheet of 2 mm. However, there is a small difference when comparing the samples, indicating that pressure did not have a significant influence on the joints.

Table 2. Geometry of the joints

Sample	Nugget Width [mm]	Nugget Height [mm]	Indentation depth h_1 (t_1) [mm]	Indentation depth h_2 (t_2) [mm]	HAZ (left) [mm]
Sample 1	6.74	1.62	0.28	0.22	0.65
Sample 2	4.80	1.82	0.21	0.16	0.51
Sample 3	6.53	1.55	0.29	0.21	0.54
Sample 4	7.49	1.93	0.27	0.20	0.73
Sample 5	7.08	2.19	0.22	0.15	0.48
Sample 6	7.21	2.07	0.25	0.22	0.55

Similar observations were reported by Kemda et al. when studying RSWs of thinner galvanised steel sheets. They observed that the welding current and time contribute in a positive way to the size of the weld nugget, while the pressing force applied by the electrodes is negligible [37]. The width of HAZ was mainly influenced by the welding current and time as well. Generally, it can be observed that the size of HAZ is directly proportional to the current.

4.3. Microstructure of the Spot-Welded Samples

Figure 9 presents the microstructure of investigated RSWs in the centre of the fusion zones. The investigated areas of all samples consist of ferrite, upper bainite, and lath martensite. The formation of upper bainite is associated with a weld time greater than 300 ms, which causes the martensite in the fusion zone to decrease and the bainite to increase. [18]. The micrographs collected using the confocal microscope in the centre of the fusion zones showed no defects, such as microcracks or pores.

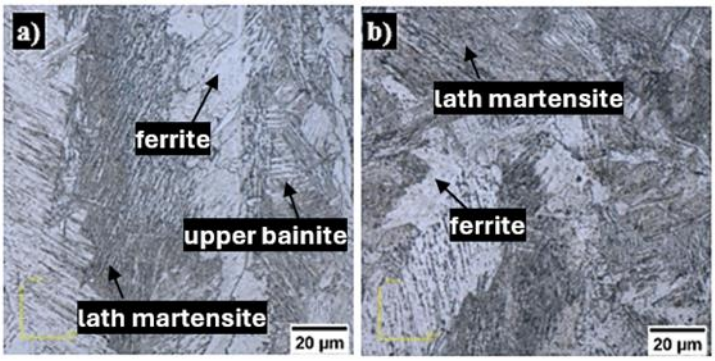

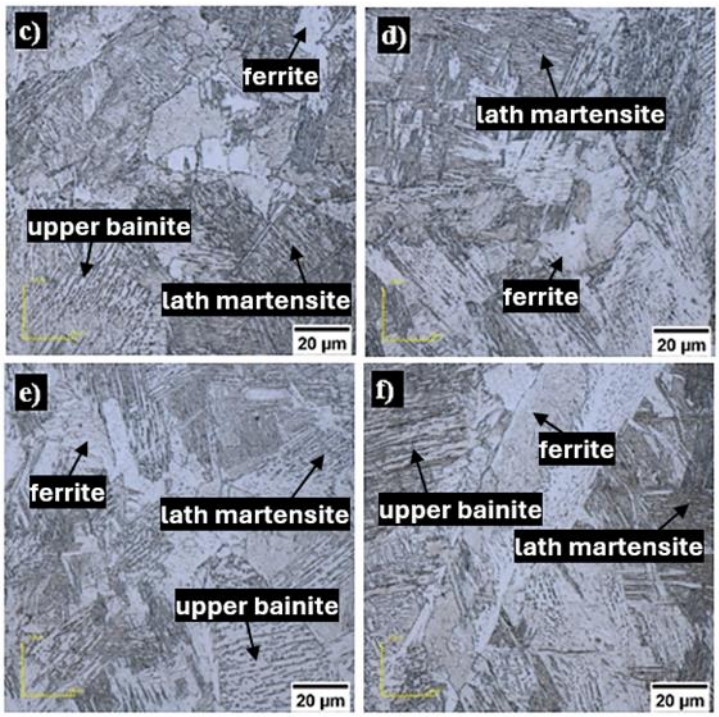

Figure 9. Microstructure of RSW in the middle of welded nuggets at 2135× magnification: a) Sample 1; b) Sample 2; c) Sample 3; d) Sample 4; e) Sample 5 and f) Sample 6

4.4. Grain Size Measurement

Figure 10 presents as a reference the nugget geometry of Sample 5 and the areas of interest for the grain size measurement labelled from 1 to 5. Every sample that was examined followed the same pattern. The centre of the nugget, the transition zone, and the upper and lower areas of the welded joint were the main subjects of our investigation.

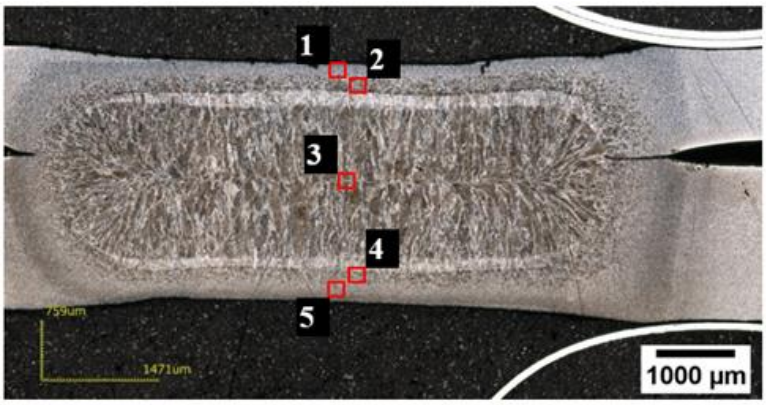

Figure 10. Nugget macrostructure of Sample 5 indicating the areas where grain size measurement was performed

The average grain size was calculated using the Line Intercept Method from micrographs taken with the confocal microscope at 2135× magnification. Five measurements were performed on three different micrographs for each sample using the ImageJ V 1.8.0 software. The average size of the grains was determined by using the following formula:

$$Average\ grain\ size = \frac{Line\ lenght}{Number\ of\ Grains} \quad (1)$$

It is well known that the microstructural characteristics of nuggets and HAZ depend on the sheet composition, the RSW temperature, the pressure, and the voltage. Table 3 presents the average grain size measured in the areas of interest such as the nugget and HAZ. When the grain sizes within a sample are compared, it can be seen that the fusion zone presents the largest grains compared to the base material. The grains in areas 1 and 5 have a finer structure compared to the base material caused by rapid cooling and recrystallisation. Areas 2 and 4 present larger grains near the fusion zone. When the fusion zones of the samples are compared, it can be seen that the grains size increases with the current caused by an increase in heat input. Gharibshahiyan et al. reported similar observations in their study, investigating the effect of current on the microstructure of low carbon steel welded using inert gas [38].

Table 3. Average grain size [µm]

Area	Sample 1	Sample 2	Sample 3	Sample 4	Sample 5	Sample 6	ASTM grain size no. G
1	6.04	7.12	7.47	6.79	4.76	4.01	12
2	8.26	9.09	10.35	10.96	9.61	6.36	12
3	18.15	20.07	20.09	20.58	23.11	20.02	8
4	9.22	8.67	9.09	7.05	8.52	5.48	12
5	3.36	4.67	4.4	4.85	3.86	3.88	12

4.5. SEM Investigation of Weld Nuggets

Based on visual inspection, Zn was not found on the surface of the RSW weld joints. This is attributed to high temperature and pressure, which generally causes the protective coating of Zn to evaporate during the welding process, as also reported by Viňáš et al. [6]. However, Zn accumulation was observed along the area surrounding the electrode indentation region, or weld shoulders, for all samples, as presented in Figure 11. In this area, zinc deposits are most likely to occur as a result of interrupted heat transfer at the weld shoulders. This is due to the fact that the electrode and the sheet are not in close contact with each other [34].

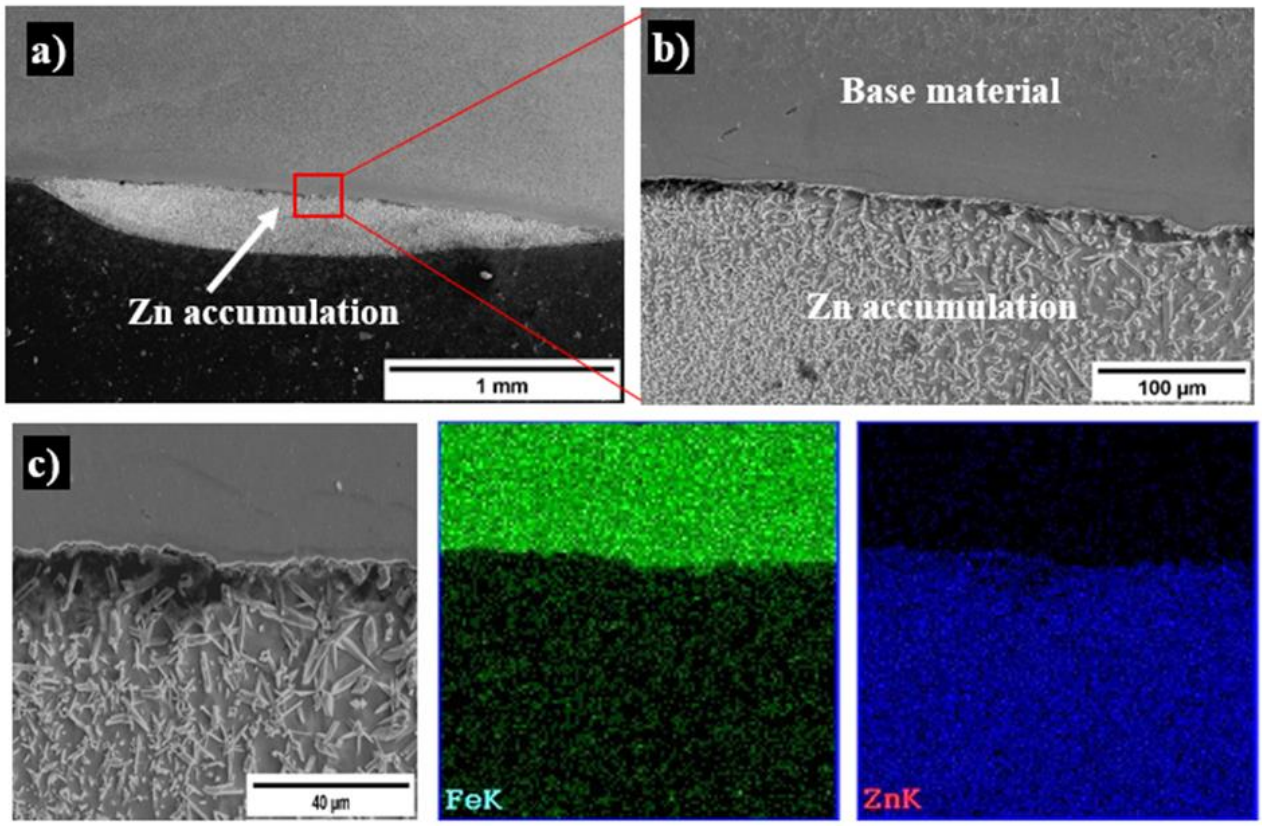

Figure 11. Region of Zn accumulation during RSW process: a) Zn accumulation at the periphery of the indentation of the electrode, b) micrographs of Zn-sheet interface and c) EDX mapping analysis of Zn-Fe

According to the SEM images presented in Figure 12, it can be observed that at higher magnification the centre of the nuggets consists of ferrite and lath martensite. The material in the fusion zone reaches high temperatures during the welding process and resolidifies very quickly, leading to a plate-like morphology [39]. Lath martensite is formed during rapid cooling in low carbon sheets and has favourable mechanical properties that depend on chemical composition and sheet thickness. The martensite transformation is considered a diffusion transformation, as carbon atoms are trapped in the matrix due to the high cooling rate followed by RSW [36]. The morphology of the martensite might be lenticular, a butterfly-thin plate, or a lath function, depending on the martensite starting temperature and carbon content. Maki et al. also reported the development of lath martensite in the fusion zone of the RSW joints [40]. However, martensite formation must be avoided or at least kept as low as possible.

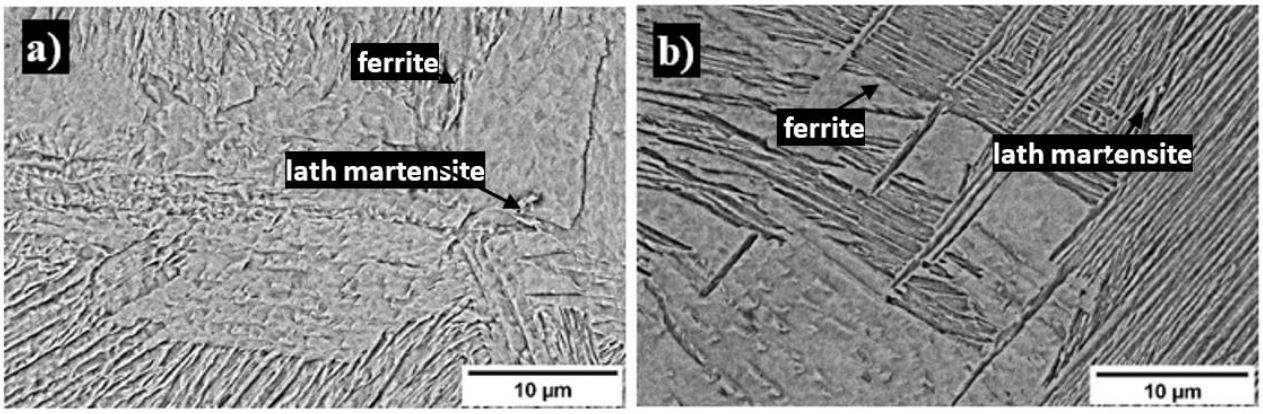

Figure 12. Representative SEM micrographs collected in the centre of the nugget at 10000× magnification: a) Sample 1 and b) Sample 5

Using SEM at higher magnification allows one to study weld imperfections in addition to macro defects and to observe defects at the microscopic level that could not be observed with the confocal microscope. A significant problem in RSW joints is cracking susceptibility, which can occur during solidification. Cracks, as presented in Figure 13-a, may serve as stress concentration sites that could lead to premature fatigue failure. Cracking in solidification is a very complex phenomenon that involves heat flow and several factors, such as welding parameters and material chemistry [41]. Since it was detected only in Sample 2, it is believed that the lower welding current and reduced force between the electrodes contributed to the formation of cracks within the nugget. Micro-cracks, especially when initiated near the fusion zone or along grain boundaries, can serve as critical stress concentrators under cyclic loading. Their presence may accelerate crack propagation during service, thereby reducing the fatigue life of the joint. This issue is particularly significant in structures exposed to dynamic loads or vibrational stresses, such as those encountered in building components, transportation frameworks, or mechanical systems utilizing lightweight steel assemblies.

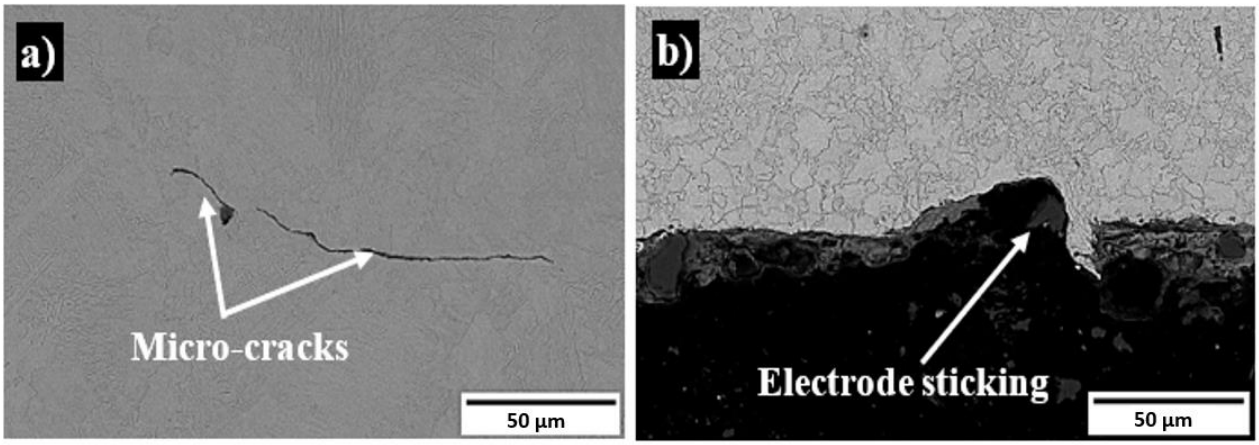

Figure 13. Weld defects a) Micro-cracks in the nugget of Sample 2 and b) effect of electrode sticking on Sample 3

Since the RWS process is fast and economical compared to other welding processes, in the present study the RSW welds were manufactured using the same electrodes. It was observed that for Sample 3, when using a current of 9627 A and a force of 4150 N between the electrodes, electrode sticking was observed as presented in Figure 13-b. Electrode sticking was not experienced for welding currents lower or above this value, although it is well-known that increasing the RSW current also increases sticking. Considering the elongated shape of the grains in the sticking area, it can be seen that the base material has a ductile behaviour, meaning that the area was not severely affected by the welding process.

From Figure 14 it can be observed that Zn not only penetrates the base material at grain boundaries but also forms grains along with Cu that come from the electrode during RSW. At the beginning of the welding process, when the electrodes are in contact with the base material and the current passes through the sample, the Zn layer is the first to melt on the contact surface. Zinc melts at 420°C and begins to boil at 906°C, which is below the melting

temperature of iron [42]. During RSW of galvanised sheets, Zn is molten and infiltrates within the weld joint at grain boundaries by capillarity due to high thermomechanical stress [43]. When infiltrated, Zn generally reacts with Fe and forms intermetallic grains, which causes weakening of the intergranular bonds leading to liquid metal embrittlement, causing a loss of toughness and ductility. From the micrographs shown in Figure 14, it is believed that Zn dissolved more easily in FCC Cu [44] (which comes from the pits removed from the rough surface of the electrode), in which case Zn has a higher affinity for Cu compared to Fe, leading to brass formation. Zn–Cu intermetallics are inherently brittle, reducing the joint's capacity to absorb repeated strain and making it more susceptible to failure especially in corrosive environments or when the temperature fluctuates. As a result, they tend to exhibit lower ductility and increased brittleness, which can reduce the joint's performance in handling micro-strain during loading cycles.

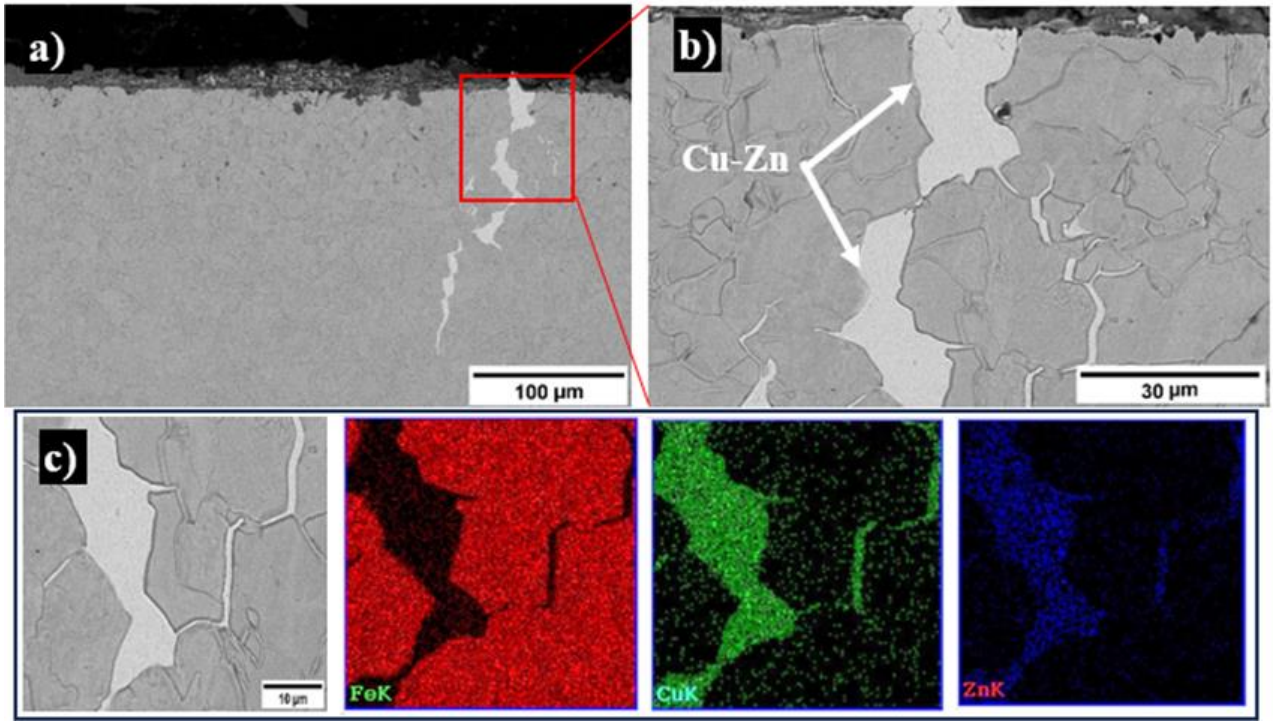

Figure 14. The cross-section in the RSW joint of Sample 4: a) Cross-section of weld with Cu-Zn contamination, b) Cu-Zn grains detected in the upper part of the weld in S250 MD with a thickness of 0.8 mm and c) EDX mapping – Fe, Cu and Zn distribution within the weld.

4.6. Nanoindentation

The microstructure, Young's modulus and hardness of the samples are directly affected by the RSW process settings, as shown by nanoindentation measurements. The load penetration curves (P-h) measured in the centre of FZ, HAZ and BM are presented in Figure 15. Among the 9 measurements performed on each area, only one typical curve is presented. The measurements performed in HAZ were collected basically in the upper-critical HAZ (UCHAZ), located next to FZ, and its microstructure consists of a coarser grain structure with constituents similar to those in the fusion zone but with an increased amount of ferrite. The maximum penetration depth for the measurements performed in the areas of interest clearly differs, indicating that the indentation response is different for HAZ and FZ compared to BM.

When comparing the first set of samples (0.8 mm joined with 1.2 mm sheet), there is no significant difference between the fusion zones, but nevertheless, a maximum penetration depth was observed for Sample 2 which had the smallest nugget diameter. On the other hand, it can be observed that there is a shift in the HAZ towards deeper values. In Sample 1 the HAZ was about 550 nm and the value increased with the increase of current up to 700 nm overlapping the value of the 0.8 mm sheet. Also, for the second set of samples (manufactured using 1.2 mm and 2 mm sheets), there is no significant difference between the measurements. However, the values of HAZ shift to deeper values, while the FZ behaves exactly the opposite when a higher welding current is employed. The measurements are influenced by phase changes and grain size distribution within the RSW joints.

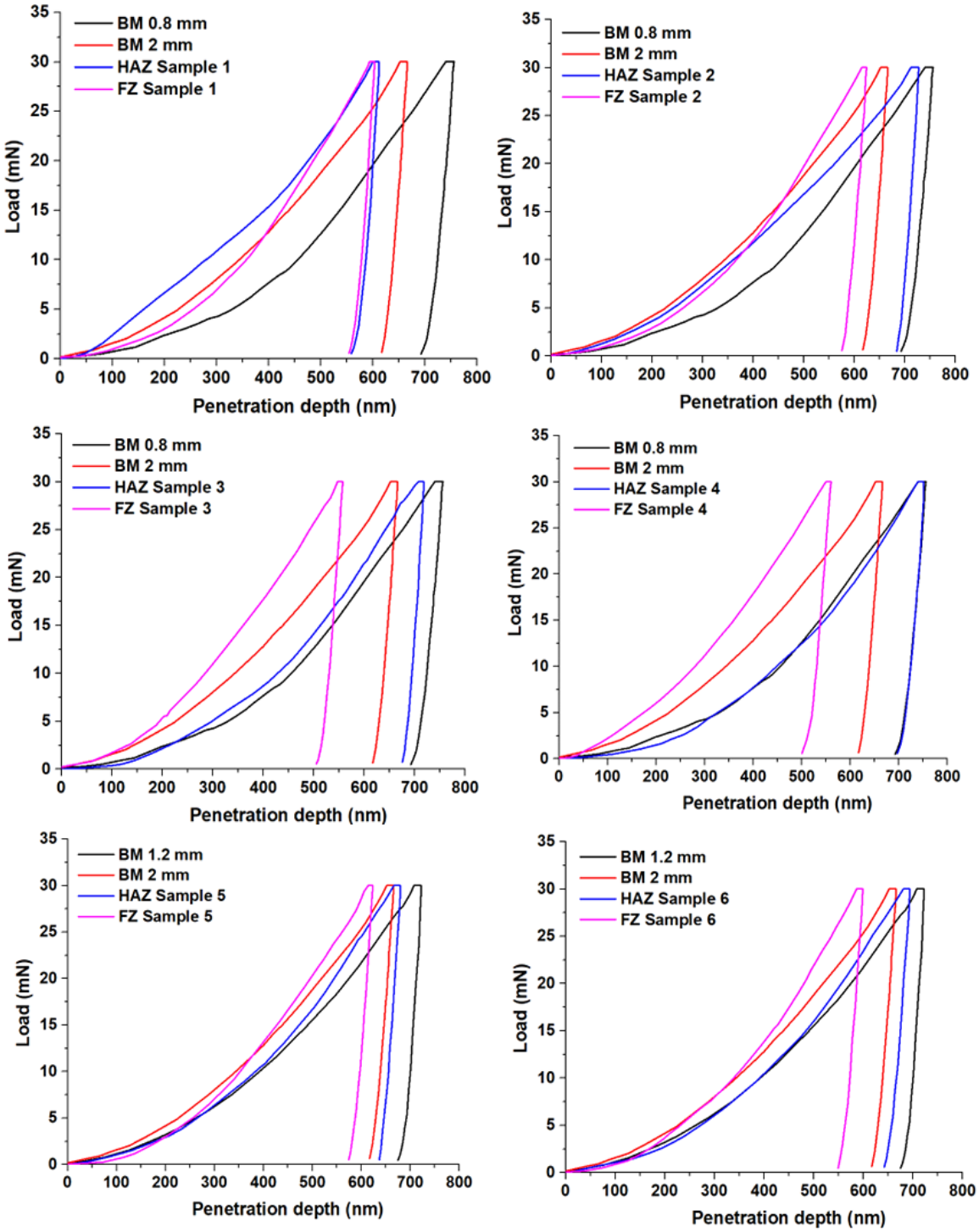

Figure 15. Representative indentation P-h curves for Samples 1-6

The elastic modulus and nanohardness values obtained by using the Oliver-Pharr analysis are presented in Table 4, where each value is an average of 9 measurements performed in HAZ and FZ, respectively. The variations of nanohardness and elastic modulus are attributed to phase changes, grain size distribution, and hardening in different areas of FZ and HAZ. As the measurement moved from the BM to the FZ, the hardness increased. The nanohardness of FZ and UCHAZ is higher in comparison with that of BM because of the formation of martensite with a lath structure and upper bainite, which have an increased hardness compared to that of ferrite. When comparing the samples, it is noticeable that the hardness increases with the welding current for the RSW joints manufactured with 0.8 mm and 2 mm sheets. This might indicate that the increase in current leads to the formation of an increased amount of martensite and bainite within the nugget. On the contrary, as the grains become coarser, the hardness values of the FZ made with sheets of 1.2 mm and 2 mm decrease as the current increases [36], which is in agreement with our grain size measurements.

Table 4. Mechanical property ranges of HAZ and FZ of Samples 1-6 (average of all 9 measured areas/sample)

Sample	Area	E [GPa]	H [GPa]
Sample 1	HAZ	283.58 ± 54.4	2.88 ± 0.47
	FZ	354.87 ± 84.43	3.22 ± 0.8
Sample 2	HAZ	284.14 ± 56.53	2.68 ± 0.42
	FZ	281.85 ± 27.06	3.15 ± 0.69
Sample 3	HAZ	301.65 ± 60.33	2.37 ± 0.39
	FZ	284.88 ± 34.36	3.11 ± 0.43
Sample 4	HAZ	320.15 ± 99.14	2.49 ± 0.98
	FZ	300.44 ± 51.45	3.33 ± 0.37
Sample 5	HAZ	274.55 ± 22.35	2.64 ± 0.49
	FZ	282.42 ± 40.05	3.37 ± 0.68
Sample 6	HAZ	289.81 ± 48.12	2.71 ± 0.38
	FZ	310.82 ± 43.62	3.28 ± 0.87

4.7. Tensile Test

The force-strain curves for the tested lap joints are presented in Figure 16. Both sets of specimens show superior capacity and ductility, as evidenced by the maximum measured force of more than 6 kN for Samples 1-4 and 12 kN for Samples 5-6. Comparing the first set of samples, a slight difference can be observed among Samples 1-4, which might be attributed to current variation and welding time. Generally, it is well known that the nugget diameter significantly affects the joint strength since a larger welded area increases the contact surface between the welded base materials, which in turn increases the strength of the welds [37]. In the present case, this was not applicable since an excessive heat input was generated at higher welding currents, and liquid metal embrittlement was noticed according to the SEM observations. Analysing the results, it can be observed that, among the RSWs manufactured using 0.8 mm and 2 mm sheets, the best weld was obtained when using 9812 A for Sample 1. On the other hand, the samples manufactured using 1.2 mm and 2 mm sheets present no significant differences. However, Samples 5 and 6 have almost double the resistance with a load of rupture highly dependent on the thickness of base materials when compared to the previously investigated samples.

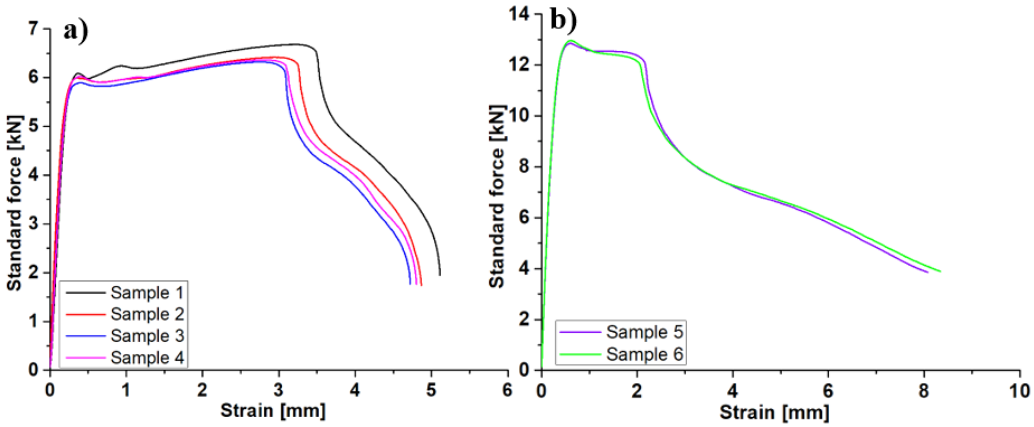

Figure 16. Force-displacement curves for: a) Samples 1-4 (0.8 with 2 mm sheets) and b) 5-6 (1.2 with 2 mm sheets)

4.8. Failure Mode

Figure 17 presents a representative macrostructure of the pull-out failure, shown in a cross-sectional view. In this failure condition, the material is ripped from one of the sheets, while the joint remains intact. All tested specimens failed by pull-out failure with the fracture propagating on the thinner sheet. In this failure mode, the fracture typically occurs in BM or HAZ. Kianersi et al. reported that an increase in welding current led to an increase in nugget size and a decrease in tensile-shear force, which might be attributed to a higher heat input. This results in joint weakness and excessive grain growth in HAZ [35].

Figure 17. Representative button pull-out failure mode encountered after the tensile tests for all the samples

In addition, an increase in welding temperature might cause a slight increase in LME (liquid metal embrittlement), which also affects the mechanical properties of the RSW-ed joints. LME induces a critical reduction in ductility and fracture strength, and it is affected, among others, by temperature, strain rate, and brittle reaction products formed in the welded areas [45, 46].

5. Conclusions

Overall, the study advances the understanding of RSW in structural applications and supports its broader implementation in the construction industry for lightweight, sustainable steel systems. In this study, lap joints were manufactured by resistance spot welding using S250GD and S350GD galvanised low-carbon steel sheets of varying thicknesses. The aim was to understand the macro- and microstructural changes caused by different welding parameters, how these parameters affect nugget formation, and their effect on mechanical properties such as hardness and tensile strength. A comparison of the results was made and led to the following conclusions:

- The built-up thin-walled cold-formed steel beams were successfully manufactured using the RSW process with galvanised low-carbon steel sheets as the base materials, making RSW a promising method for lightweight steel constructions;
- The weld region is comprised of three main structural zones which are (i) the base metal, (ii) the heat-affected zone, and (iii) the nugget/fusion zone. Their dimensions are closely correlated to the welding parameters. As the value of the welding current increases, the diameter of the nugget increases as well. Thus, a high heat input increases weld nugget deformation as a result of increased electrode penetration depth into the base material, while the size of HAZ is directly proportional to the current;
- The microstructure of the samples consists of ferrite and lath martensite. Additionally, upper bainite was identified. Its presence is due to fast cooling and a longer welding time, which lead to a reduction of martensite and an increase in bainite within the fusion zone;
- The fusion zones of the samples present the largest grains within the joint, and when comparing the samples, the different grain sizes found within the nuggets are attributed to an increased heat input that comes with an increased current leading to grain growth;
- Higher heat input increases nugget diameter but may also cause micro-defects such as micro-cracks and electrode sticking, which were revealed along Zn-Cu intermetallics, emphasising the need for precise control of welding conditions;
- The variations in hardness and Young's modulus are attributed to phase changes, grain size distribution, hardening in different areas of the melt zone and heat-affected zone. The hardness of the nugget is higher than that of the base material due to the formation of martensite with lath structure and upper bainite, which have increased hardness compared to ferrite;
- Both sets of samples have good capacity and ductility; however, excessive martensite can reduce ductility. Slight differences were observed, which are attributed to the current and welding time variations;
- Tensile testing confirmed strong, ductile joints with failure in the base material, not in the weld. All tested specimens failed by full button pull-out with the fracture propagated on the thinner sheet;
- From the first set of samples, Sample 1 presented the best mechanical properties, indicating that optimal parameters for 0.8 mm and 2 mm sheets were 9812 A, 4300 N, and 446 ms. The second set of samples exhibited better mechanical properties than the first, and only slight differences were noted when comparing the performance of Sample 5 with Sample 6.

6. Declarations

6.1. Author Contributions

Conceptualization, I.H. and V.U.; methodology, V.U.; software, I.H.; validation, R.B., I.B., and E.P.; formal analysis, V.U.; investigation, I.H., V.U., R.B., and I.B.; resources, V.U.; data curation, I.H.; writing—original draft preparation, I.H.; writing—review and editing, V.U., E.P., and R.B.; visualization, R.B. and I.B.; supervision, V.U.; project administration, V.U.; funding acquisition, V.U. All authors have read and agreed to the published version of the manuscript.

6.2. Data Availability Statement

The data presented in this study are available on request from the corresponding author.

6.3. Funding

This work was supported by a grant of the Romanian Ministry of Research and Innovation, CCCDI-UEFISCDI, project number PN-III-P2-2.1-PTE-2021-0237-Wellformed-Frames, within PNCDI III.

6.4. Conflicts of Interest

The authors declare no conflict of interest.

7. References

[1] Li, M., Tao, W., Zhang, J., Wang, Y., & Yang, S. (2022). Hybrid resistance-laser spot welding of aluminum to steel dissimilar materials: Microstructure and mechanical properties. Materials and Design, 221, 111022. doi:10.1016/j.matdes.2022.111022.

[2] Ashiri, R., Mostaan, H., & Park, Y. Do. (2018). A Phenomenological Study of Weld Discontinuities and Defects in Resistance Spot Welding of Advanced High Strength TRIP Steel. Metallurgical and Materials Transactions A: Physical Metallurgy and Materials Science, 49(12), 6161–6172. doi:10.1007/s11661-018-4900-0.

[3] Adkine, A. S., & Biradar, S. K. (2024). A review of the effects of resistance spot welding on metallurgical and mechanical characteristics. Welding International, 39(2). doi:10.1080/09507116.2024.2419551.

[4] Rao, S. S., Chhibber, R., Arora, K. S., & Shome, M. (2017). Resistance spot welding of galvannealed high strength interstitial free steel. Journal of Materials Processing Technology, 246, 252–261. doi:10.1016/j.jmatprotec.2017.03.027.

[5] Biradar, A. K., & Dabade, B. M. (2019). Optimization of resistance spot welding process parameters in dissimilar joint of MS and ASS 304 sheets. Materials Today: Proceedings, 26, 1284–1288. doi:10.1016/j.matpr.2020.02.256.

[6] Viňáš, J., Kaseak, L., & Greš, M. (2016). Optimization of resistance spot welding parameters for microalloyed steel sheets. Open Engineering, 6(1), 504–510. doi:10.1515/eng-2016-0069.

[7] Emre, H. E., & Kaçar, R. (2016). Resistance spot weldability of galvanize coated and uncoated TRIP steels. Metals, 6(12), 299. doi:10.3390/met6120299.

[8] Hamidinejad, S. M., Kolahan, F., & Kokabi, A. H. (2012). The modeling and process analysis of resistance spot welding on galvanized steel sheets used in car body manufacturing. Materials and Design, 34, 759–767. doi:10.1016/j.matdes.2011.06.064.

[9] Chao, Y. J. (2003). Ultimate strength and failure mechanism of resistance spot weld subjected to tensile, shear, or combined tensile/shear loads. Journal of Engineering Materials and Technology, 125(2), 125–132. doi:10.1115/1.1555648.

[10] Radakovic, D. J., & Tumuluru, M. (2008). Predicting resistance spot weld failure modes in shear tension tests of advanced high-strength automotive steels. Welding Journal (Miami, Fla), 87(4), 96–105.

[11] Pouranvari, M., Marashi, P., Goodarzi, M., & Abedi, A. (2008). An analytical model predicting failure mode of resistance spot welds. 17th International Conference on Metallurgy and Materials, Ostrava, Czechia.

[12] Miyazaki, Y., & Furusako, S. (2007). Tensile shear strength of laser welded lap joints. Nippon Steel Technical Report, 95, 28-34.

[13] Landolfo, R., Mammana, O., Portioli, F., Di Lorenzo, G., & Guerrieri, M. R. (2008). Laser welded built-up cold-formed steel beams: Experimental investigations. Thin-Walled Structures, 46(7–9), 781–791. doi:10.1016/j.tws.2008.03.009.

[14] Kodama, S., Furusako, S., Miyazaki, Y., Ishida, Y., Saito, M., & Nose, T. (2013). Arc welding technology for automotive steel sheets. Nippon Steel Technical Report, 103(103), 83–90.

[15] Jeffus, L. (2011). Welding: Principles and Applications. (7th Ed.). Cengage Learning, Boston, United States.

[16] Podržaj, P., Polajnar, I., Diaci, J., & Karič, Z. (2006). Influence of welding current shape on expulsion and weld strength of resistance spot welds. Science and Technology of Welding and Joining, 11(3), 250–254. doi:10.1179/174329306X101391.

[17] Yi, L., Rui, W., Xiaojian, X., & Yang, Z. (2016). Expulsion analysis of resistance spot welding on zinc-coated steel by detection of structure-borne acoustic emission signals. International Journal of Advanced Manufacturing Technology, 84(9–12), 1995–2002. doi:10.1007/s00170-015-7846-z.

[18] Marashi, P., Pouranvari, M., Amirabdollahian, S., Abedi, A., & Goodarzi, M. (2008). Microstructure and failure behavior of dissimilar resistance spot welds between low carbon galvanized and austenitic stainless steels. Materials Science and Engineering: A, 480(1–2), 175–180. doi:10.1016/j.msea.2007.07.007.

[19] Zhang, W. H., Qiu, X. M., Sun, D. Q., & Han, L. J. (2011). Effects of resistance spot welding parameters on microstructures and mechanical properties of dissimilar material joints of galvanised high strength steel and aluminium alloy. Science and Technology of Welding and Joining, 16(2), 153–161. doi:10.1179/1362171810Y.0000000009.

[20] Májlinger, K., Katula, L. T., & Varbai, B. (2023). Global Approach on the Shear and Cross Tension Strength of Resistance Spot Welded Thin Steel Sheets. Periodica Polytechnica Mechanical Engineering, 67(4), 315–339. doi:10.3311/ppme.23184.

[21] Yang, K., Meschut, G., Seitz, G., Biegler, M., & Rethmeier, M. (2023). The Identification of a New Liquid Metal Embrittlement (LME) Type in Resistance Spot Welding of Advanced High−Strength Steels on Reduced Flange Widths. Metals, 13(10), 1754. doi:10.3390/met13101754.

[22] Yang, K., Sowada, M., Olfert, V., Seitz, G., Schreiber, V., Heitmann, M., Hein, D., Biegler, M., Jüttner, S., Rethmeier, M., & Meschut, G. (2024). Influence of liquid metal embrittlement on the failure behavior of dissimilar spot welds with advanced high-strength steel: A component study. Journal of Materials Research and Technology, 33, 8321–8328. doi:10.1016/j.jmrt.2024.11.166.

[23] Sun, Y., Zhou, J., Hu, R., Pan, H., Ding, K., Lei, M., & Gao, Y. (2024). The High-Cycle Tensile–Shear Fatigue Properties and Failure Mechanism of Resistance Spot-Welded Advanced High-Strength Steel with a Zn Coating. Materials, 17(18), 4463. doi:10.3390/ma17184463.

[24] Hagen, C., Klinkenberg, F. J., Ossenbrink, R., & Michailov, V. (2023). Resistance spot welding of dissimilar material joints with a cold-gas-sprayed inlayer. International Journal of Advanced Manufacturing Technology, 127(11–12), 5679–5690. doi:10.1007/s00170-023-11897-x.

[25] Wang, G., Zhou, K., Ren, B., & Yu, W. (2025). Influence of Cu/Ni coating on microstructure and mechanical properties in steel/aluminum single-sided resistance spot welding joint. Journal of Materials Processing Technology, 335, 118675. doi:10.1016/j.jmatprotec.2024.118675.

[26] Yang, K., Wang, Z., Haak, V., Olfert, V., El-Sari, B., Hein, D., Biegler, M., Rethmeier, M., & Meschut, G. (2025). A novel welding schedule for expanding the expulsion-free process window in resistance spot welding of dissimilar joints with ultra-high strength steel. Journal of Manufacturing Processes, 137, 306–319. doi:10.1016/j.jmapro.2025.02.009.

[27] Ullrich, M., Wohner, M., & Jüttner, S. (2024). Quality monitoring for a resistance spot weld process of galvanized dual-phase steel based on the electrode displacement. Welding in the World, 68(7), 1791–1800. doi:10.1007/s40194-024-01720-w.

[28] Asati, B., Bag, S., Shajan, N., Kadarbhai, M. A., Singh, P., Arora, K. S., & Singh, A. P. (2024). Tailoring Electrode Life Expectancy in Pre-pulse Resistance Spot Welding of Coated High-Strength Interstitial Free Steel. Journal of Materials Engineering and Performance. doi:10.1007/s11665-024-09721-y.

[29] Özen, F., Onar, V., Bulca, M., & Aslanlar, S. (2023). Resistance spot weldability of Fe-15.4Mn-2.1Al-1.2C twinning induced plasticity steel. Materialwissenschaft Und Werkstofftechnik, 54(7), 857–870. doi:10.1002/mawe.202200241.

[30] Niemiro-Maźniak, J., & Lacki, P. (2024). Experimental and numerical analysis of joints and thin-walled steel beams fabricated through resistance spot welding and hot-dip galvanizing. Thin-Walled Structures, 202, 112105. doi:10.1016/j.tws.2024.112105.

[31] Fawzy, K., Moustafa, A., & Farouk, M. A. (2024). Innovative reinforcement techniques for optimizing the performance of shallow, wide beams in reinforced concrete structures. Innovative Infrastructure Solutions, 9(10), 395. doi:10.1007/s41062-024-01708-x.

[32] Ungureanu, V., Both, I., Burca, M., Radu, B., Neagu, C., & Dubina, D. (2021). Experimental and numerical investigations on built-up cold-formed steel beams using resistance spot welding. Thin-Walled Structures, 161. doi:10.1016/j.tws.2021.107456.

[33] Muhammad, N., Manurung, Y. H., Hafidzi, M., Abas, S. K., Tham, G., & Rahim, M. R. A. (2012). A Quality Improvement Approach for Resistance Spot Welding using Multi-objective Taguchi Method and Response Surface Methodology. International Journal on Advanced Science, Engineering and Information Technology, 2(3), 215. doi:10.18517/ijaseit.2.3.189.

[34] Bhattacharya, D. (2018). Liquid metal embrittlement during resistance spot welding of Zn-coated high-strength steels. Materials Science and Technology (United Kingdom), 34(15), 1809–1829. doi:10.1080/02670836.2018.1461595.

[35] Kianersi, D., Mostafaei, A., & Amadeh, A. A. (2014). Resistance spot welding joints of AISI 316L austenitic stainless-steel sheets: Phase transformations, mechanical properties and microstructure characterizations. Materials and Design, 61, 251–263. doi:10.1016/j.matdes.2014.04.075.

[36] Pawar, S., Singh, A. K., Kaushik, L., Park, K. S., Shim, J. H., & Choi, S. H. (2022). Characterizing local distribution of microstructural features and its correlation with microhardness in resistance spot welded ultra-low-carbon steel: Experimental and finite element characterization. Materials Characterization, 194, 112382. doi:10.1016/j.matchar.2022.112382.

[37] Feujofack Kemda, B. V., Barka, N., Jahazi, M., & Osmani, D. (2020). Optimization of resistance spot welding process applied to A36 mild steel and hot dipped galvanized steel based on hardness and nugget geometry. International Journal of Advanced Manufacturing Technology, 106(5–6), 2477–2491. doi:10.1007/s00170-019-04707-w.

[38] Gharibshahiyan, E., Raouf, A. H., Parvin, N., & Rahimian, M. (2011). The effect of microstructure on hardness and toughness of low carbon welded steel using inert gas welding. Materials and Design, 32(4), 2042–2048. doi:10.1016/j.matdes.2010.11.056.

[39] Lee, H. T., & Chang, Y. C. (2020). Effect of double pulse resistance spot welding process on 15B22 hot stamped boron steel. Metals, 10(10), 1–17. doi:10.3390/met10101279.

[40] Maki, T. (2012). Morphology and substructure of martensite in steels. Phase Transformations in Steels, 2, 34–58. doi:10.1533/9780857096111.1.34.

[41] Aucott, L., Huang, D., Dong, H. B., Wen, S. W., Marsden, J. A., Rack, A., & Cocks, A. C. F. (2017). Initiation and growth kinetics of solidification cracking during welding of steel. Scientific Reports, 7(1), 40255. doi:10.1038/srep40255.

[42] Zhu, Y., Wang, H. P., Wang, Y., Hao, Y., Carlson, B. E., & Lu, F. (2021). Formation mechanism of liquid metal embrittlement in laser lap welding of zinc-coated GEN3 steels. Materials Science and Engineering: A, 800. doi:10.1016/j.msea.2020.140229.

[43] Lee, H., Jo, M. C., Sohn, S. S., Kim, S. H., Song, T., Kim, S. K., Kim, H. S., Kim, N. J., & Lee, S. (2019). Microstructural evolution of liquid metal embrittlement in resistance-spot-welded galvanized TWinning-Induced Plasticity (TWIP) steel sheets. Materials Characterization, 147, 233–241. doi:10.1016/j.matchar.2018.11.008.

[44] Hong, H. L., Wang, Q., Dong, C., & Liaw, P. K. (2014). Understanding the Cu-Zn brass alloys using a short-range-order cluster model: Significance of specific compositions of industrial alloys. Scientific Reports, 4, 7065. doi:10.1038/srep07065.

[45] Razmpoosh, M. H., Biro, E., Chen, D. L., Goodwin, F., & Zhou, Y. (2018). Liquid metal embrittlement in laser lap joining of TWIP and medium-manganese TRIP steel: The role of stress and grain boundaries. Materials Characterization, 145, 627–633. doi:10.1016/j.matchar.2018.09.018.

[46] Kim, D., Kang, J. H., & Kim, S. J. (2018). Heating rate effect on liquid Zn-assisted embrittlement of high Mn austenitic steel. Surface and Coatings Technology, 347, 157–163. doi:10.1016/j.surfcoat.2018.04.081.